

Analysis of Turbulent Flame Propagation in Equivalence Ratio-Stratified Flow

Edward S. Richardson^{*1} and Jacqueline H. Chen²

¹Faculty of Engineering and the Environment
University of Southampton
Southampton, SO17 1BJ, United Kingdom

²Combustion Research Facility
Sandia National Laboratories
Livermore, CA 94551-0969, USA

Abstract

Effects of equivalence ratio stratification on turbulent combustion processes are investigated using Direct Numerical Simulation. The simulation results are analysed in terms of flame surface area and the burning intensity. The local effects of stratification are then investigated further by examining statistics of the displacement speed conditioned on the flame-normal equivalence ratio gradient. The local burning intensity is found to depend on the orientation of the stratification with respect to the flame front, so that burning intensity is enhanced when the flame speed in the products is faster than in the reactants. The flame surface area is also influenced by equivalence ratio stratification and this may be explained by differences in the surface averaged consumption speed and differential propagation effects due to flame speed variations associated with equivalence ratio fluctuations.

Introduction

A wide range of practical combustion devices involve flame propagation in fuel-air mixtures which are not perfectly mixed. This study focusses on equivalence ratio-stratified combustion, in which a flame propagates through an inhomogeneous fuel-air mixture. Understanding and predictive modelling for equivalence ratio-stratified combustion physics are important for the design of stratified-charge internal combustion engines as well as lean-burn gas turbine combustion systems.

Turbulent premixed combustion has been described phenomenologically as a propagating flame surface which is distorted by its interactions with the turbulent flow [1]. According to this description, the turbulent flame speed of a homogeneous mixture, S_T , will differ from the laminar flame speed S_L , according to,

$$\frac{S_T}{\langle S_L \rangle_s} = I_0 A' \quad (1)$$

where A' is the ratio of the turbulent flame area A_{turb} divided by the projected frontal area of the flame, A ,

$$A' = \frac{A_{turb}}{A}, \quad (2)$$

and the burning intensity I_0 is the ratio of the surface averaged displacement speed to the surface averaged laminar flame speed, $\langle S_L(\varphi) \rangle_s$. The laminar flame speed is surface averaged in this presentation because, in equivalence ratio stratified flows, S_L depends on the local value of the spatially-varying equivalence ratio, $\varphi(\mathbf{x})$. Describing stratified combustion with Eq. 1 raises two major questions: first, how does stratification influence the flame surface area in a turbulent flame; and second,

how does stratification influence the burning intensity? The objective of this study is to address both of these questions by examining new DNS data for turbulent stratified combustion with realistic methane-air chemistry.

Previous theoretical and numerical studies suggest that fluctuations of the local flame speed due to equivalence-ratio stratification provide a mechanism for wrinkling the flame, described as a *differential propagation* [2]. Whether the differential propagation mechanism has a significant impact on the turbulent flame speed depends on the magnitude of the flame speed fluctuations S_L'/\bar{S}_L [2] and the length scale of the equivalence ratio fluctuations [3,4]: it has been suggested that differential propagation can be significant for $S_L' \sim u'$ [2] at stratification length scales between the integral scale and the scale where scalar dissipation timescale competes with the flame propagation timescale [5,6]. However flame surface density-based modelling approaches have been assessed in equivalence-ratio stratified flames and have achieved moderate success without considering effects of differential propagation [7,8].

The effect of equivalence ratio variation on the local burning intensity has not been investigated in turbulent flame simulations with realistic chemistry. It has been found that flame-normal equivalence ratio gradients affect the propagation speed of laminar flames, due to the effect of equivalence ratio gradients on the molecular transport of radical species and hot products into the reaction zone [9]. It has been observed that *back-supported* flames yield higher propagation speed than flames in homogenous mixture, and that flames in homogeneous mixture yield faster propagation speed than *front-supported* flames. The terms back-supported and front-supported describe flames in which the laminar

* Corresponding author: e.s.richardson@soton.ac.uk

flame speed on the product side of the flame is greater and less, respectively, than in the reactants. The present DNS study examines the impacts of differential propagation and front/back-support effects in turbulent flames simulated with realistic chemistry.

Equivalence ratio-stratified DNS

Simulation configuration: Effects of equivalence ratio stratification on turbulent combustion processes are investigated using Direct Numerical Simulation (DNS). The simulation configuration involves a slot-jet turbulent Bunsen flame that is periodic in the span-wise z -direction (the coordinate system is indicated in Figure 1). Four cases (C1, C2, C4, C5) are considered that all have a mean equivalence ratio equal to 0.7, but different equivalence ratio stratification: C1, a perfectly-premixed Bunsen flame with equivalence ratio 0.7 reported in previous studies [10,11,12]; C2, a tangentially-stratified Bunsen flame configuration shown in Figure 1 with equivalence ratio variation from 0.41-1.0; C4 and C5, *back-supported* and *front-supported* flames with equivalence ratio varying from 0.41-1.0 and 1.0-0.41 between the reactants and products respectively as shown in Figure 1.

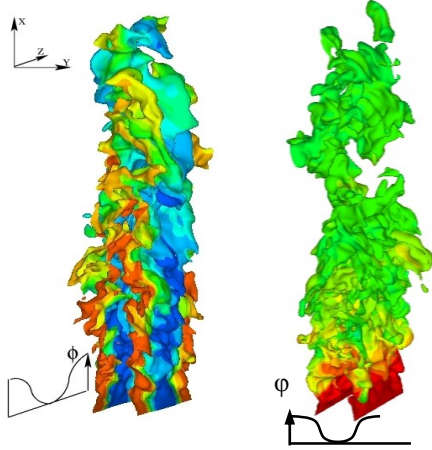


Figure 1. Instantaneous $c=0.5$ iso-surface coloured by case mixture fraction Z (blue=0, red=1): left, case C2; right case C4.

The *fuel-air* mixture fraction ξ , which equals zero in pure air and unity in pure methane, is linearly related to the *case* mixture fraction Z .

$$\xi = \xi_0 + Z(\mathbf{x})(\xi_1 - \xi_0) \quad (3)$$

Z is defined as a conserved scalar with unity Lewis number, taking a value equal to zero at the minimum fuel-air mixture fraction ξ_0 in each case, and unity at the maximum value of fuel-air mixture fraction, ξ_1 . A temperature-based progress variable is defined using the oxygen mass fraction and normalised by the burnt and unburnt compositions as a function of mixture fraction,

$$c_T = \frac{T - T_u(\xi)}{T_b(\xi) - T_u(\xi)}. \quad (4)$$

$T_b(\xi)$ is the product temperature at the local value of ξ , and $T_u(\xi)$ is the unburnt temperature, which is equal to 800K in all cases.

The slot jet width H is 1.8mm, the jet velocity U_j is 100ms^{-1} and the coflow velocity U_c is 25ms^{-1} giving a jet Reynolds number of 2100 based on the kinematic viscosity in the unburned mixture ($8.5 \times 10^{-5} \text{m}^2 \text{s}^{-1}$). The inlet profiles of Z , c_T , and velocity \mathbf{u} are prescribed by Eqs. 5-9.

$$c_T(y, z) = 1 - \frac{1}{4} \left(1 - \tanh \left[\frac{2y - (H + 3\delta)}{\delta} \right] \right) \cdot \left(1 - \tanh \left[\frac{2y + (H + 3\delta)}{\delta} \right] \right) \quad (5)$$

where $\delta = 0.3$ mm is representative of the flame thickness at the conditions employed. The fuel-air mixture fraction for case C1 is uniform and equal to 0.03928 (i.e. $\phi=0.7$). The periodic span-wise variation of mixture fraction for case C2 is given by

$$Z(y, z) = 1 - \frac{1}{4} \left(1 - \tanh \left[\frac{z - 0.75L_z}{H/2} \right] \right) \cdot \left(1 - \tanh \left[\frac{z - 0.25L_z}{H/2} \right] \right) \quad (6)$$

where $L_z = 4H$ is the length of the simulation domain in the span-wise z -direction. In case C4 the case mixture fraction varies in the transverse y -direction

$$Z(y, z) = 1 - \frac{1}{4} \left(1 - \tanh \left[\frac{2y - (H + n\delta)}{\delta} \right] \right) \cdot \left(1 - \tanh \left[\frac{2y + (H + n\delta)}{\delta} \right] \right) \quad (7)$$

The mixture fraction in case C5 varies in the opposite direction from case C4 and it is given by one minus the value from Eq. 7. The values of n determine the spatial offset between the mixture fraction and progress variable profiles: $n = 0$ in case C4 and $n = 3$ in case C5. The values of n were selected so that the flame and the equivalence ratio mixing layer intersect within the domain.

The mean inlet velocity in case C1 is given by,

$$\tilde{U}_{C1}(y) = U_c + \frac{1}{2}(U_j - U_c) \left(\tanh \left[\frac{2y + 0.85H}{0.05H} \right] - \tanh \left[\frac{2y - 0.85H}{0.05H} \right] \right) \quad (8)$$

The inflow velocities in the stratified cases are then scaled by the ratio between the local density and the corresponding density in the perfectly premixed C1 case in order to obtain the same mass flow rate per unit area,

$$\tilde{U}(y, z) = \frac{\tilde{U}_{C1}(y)\rho_{C1}(y)}{\rho(x, y)}. \quad (9)$$

The mass fractions and temperature at the inlet boundary are obtained from laminar flame data tabulated as a function of the mixture fraction and progress variable given by Eqs. 5-7. The laminar flame simulations use the same thermo-chemical models as the turbulent DNS. The look-up table for flame C1 was generated from a freely propagating planar premixed laminar flame solution at $\phi = 0.7$. The look-up tables for the equivalence ratio-stratified flames were obtained from two-dimensional laminar flame simulations of a flame propagating into a mixing layer. The two-dimensional flames are anchored at the inflow boundary by a co-flow of products on both sides of the mixing layer. The simulation domain was $10\text{mm} \times 16\text{mm}$; the inflow velocity was uniform and equal to 3ms^{-1} ; and the distance between the co-flowing product streams was 2.1mm , resulting in a stationary flame shown in Figure 2.

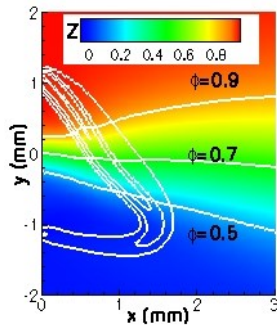


Figure 2. Temperature distribution in the laminar flame simulation used to obtain $Z - c_T$ look-up table, with iso-lines of heat release rate and equivalence ratio indicated.

Pseudo-turbulent velocity fluctuations are superimposed on the mean jet flow at the inlet boundary, and the fluctuation amplitude is set to zero in the coflow. A field of homogeneous isotropic divergence-free velocity fluctuations was generated with a prescribed kinetic energy spectrum [13]. The field of velocity fluctuations are fed into the domain with the mean jet velocity. The integral length scales are $2H$ for cases C1, C4 and C5, and $1.33H$ for case C2, and the rms velocity fluctuation is $U_j/3$ for cases C1, C4, C5 and $U_j/4$ for case C2.

Physical models: Chemical reaction is modelled using a reduced mechanisms with low temporal stiffness, consisting of 13-species and 9-steps, as used previously by Sankaran et al. [11]. Thermal conductivity is modelled as a function of temperature and heat capacity [14]. The Prandtl number is assumed constant and equal to 0.708. Constant Lewis number transport is assumed with species Lewis numbers obtained by averaging the mixture-averaged diffusivities in a $\phi = 0.7$ premixed flame. The species retained in the kinetic mechanism, and their Lewis numbers are listed in Table 1.

Table 1. Lewis numbers used in the DNS

H_2	H	O	O_2	OH	H_2O	HO_2
0.29	0.17	0.69	1.08	0.70	0.82	1.07
CH_3	CH_4 :	CO :	CO_2	CH_2O	N_2	Z
0.97	0.96	1.07	1.354	1.25	1.04	1.00

Numerical methods: The simulations were performed using Sandia’s *S3D* DNS code [15], which solves the compressible Navier Stokes, species, and energy equations with a fourth order Runge-Kutta method for time integration and eighth-order explicit spatial differencing [16,17]. The computational domain extends to $L_x = 13.3H$ in the stream-wise direction and in the cross-stream direction $L_y = \pm 6H$ for cases C1 and C2, and $L_y = \pm 7H$ for cases C4-C5. For case C1 the extent of the periodic z -direction is $L_z = 3H$, while for all of the stratified cases the span-wise extent is $L_z = 4H$. A uniform $20\mu\text{m}$ grid spacing was employed throughout the volume occupied by the turbulent jet flame. The grid in the transverse direction was stretched algebraically in the laminar coflow. Case C2 is discretised with $1200 \times 600 \times 360 = 259$ Million grid points. The premixed and stratified simulations were advanced with 2ns and 4ns time steps respectively. Further details of the configuration are given in Refs. [11,12]. Navier Stokes Characteristic Boundary Conditions [18] were used at the non-periodic boundaries.

Results

Previous analysis [11,12] shows that premixed case C1 is characterised by the thin-reaction zones regime, with turbulent mixing acting to thicken the preheat zone of the flame. The turbulent combustion parameters reported in Table 2 are evaluated on the jet centre-line at one half of the domain height. The Karlovitz number $(\alpha/S_L l_k)$ depends on the thermal diffusivity in the reactants $\alpha = 1.2 \times 10^{-4} \text{m}^2\text{s}^{-1}$, the laminar flame speed, and the Kolmogorov length scale, $l_k = (\nu^3/\bar{\epsilon})^{1/4}$, where the kinematic viscosity $\nu = 8.5 \times 10^{-5} \text{m}^2\text{s}^{-1}$ in the unburned reactants, and $\bar{\epsilon}$ is the mean turbulent kinetic energy dissipation rate. The turbulent length scale $L_T = u'^3/\bar{\epsilon}$, where u' is the root mean square velocity fluctuation. The Karlovitz number is greater than unity for all of the mixtures encountered, indicating that the stratified flames are also in the thin reaction zones regime, and the Karlovitz number Ka_δ based on the full-width at half maximum thickness of the heat release profile δ_H is approximately equal to 15 for the leanest mixture – positioning the leanest part of the flame in the broken reaction zones regime according to the premixed regime diagram [19].

Table 2. Combustion parameters for premixed case C1 and stratified cases C4 and C5.

	Premixed	Stratified
ϕ	0.7	0.41-1.0
$S_L (\text{ms}^{-1})$	1.8	0.6-2.5
$\delta_L (\text{mm})$	0.29	0.46-0.26
u'/S_L	5.4	16.-3.9
L_T/δ_L	1.7	1.1-2.0
$Ka = (\alpha/S_L l_k)$	7.6	69-3.9
$Ka_\delta = Ka \cdot (\delta_H/\delta_L)^2$	1.7	15.-0.9

Figure 3 and Figure 4 show the stream-wise variation of the normalised flame surface area A' , burning intensity I_0 , and the turbulent and laminar consumption rates for

case C1, C4 and C5 (Figure 3) and for case C2 (Figure 4). Noting that the flame brush is approximately normal to the y -direction and, away from the tip of the flame, that the flame brush is crossed twice in the range $-\infty < y < \infty$, turbulent flame properties are obtained by integration in the y - z plane,

$$\psi_{turb} = \frac{1}{2(z_2 - z_1)} \int_{z_1}^{z_2} \int_{-\infty}^{\infty} \psi \cdot dy \cdot dz. \quad (10)$$

Cases C1, C4 and C5 are statistically homogeneous in the span-wise z -direction and the range of integration, $z_2 - z_1$, is equal to the span of the domain, L_z . Equivalence ratio varies across the span of the C2 case and the turbulent flame properties are evaluated at three span-wise locations $L_z = 0.0, 0.25$, and 0.5 , corresponding to mean equivalence ratios of $\bar{\varphi} = 1.0, 0.7$ and 0.41 , approximately.

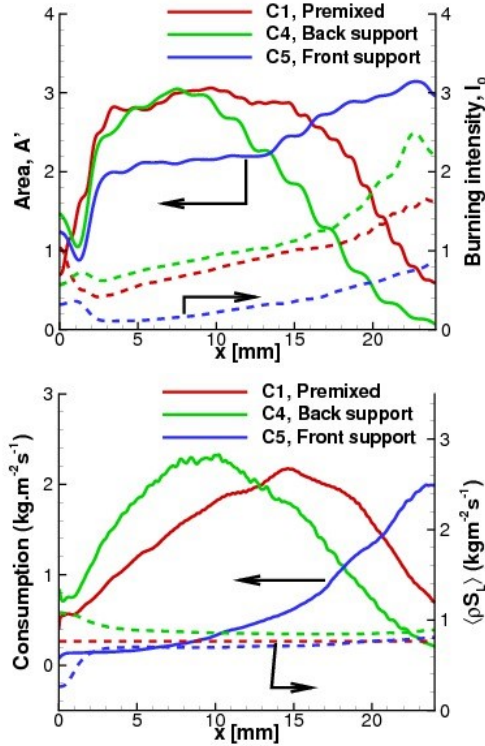


Figure 3. Stream-wise variation of turbulent flame properties in cases C1, C4, and C5.

The normalised flame surface area A' is obtained by integrating the magnitude of the cross-stream gradient of progress variable, $\psi = |\nabla c|$. Following Refs. [11,12] the simulations have been analysed using a progress variable c defined analogously to Eq. 4, but in terms of O_2 mass fraction. It has been verified that there is a monotonic relationship between c_T and c at constant Z throughout the $Z - c_T$ look-up table. The turbulent consumption rate is calculated by substituting $\psi = -\dot{\omega}_{O_2} / (Y_{O_2,u}(\xi) - Y_{O_2,b}(\xi))$, where $\dot{\omega}_{O_2}$ is the reaction rate (in $\text{kg}\cdot\text{m}^{-3}\cdot\text{s}^{-1}$) for O_2 and $Y_{O_2,u}$ and $Y_{O_2,b}$ are the mass fraction of O_2 in the unburned and burned mixture as a function of the local value of ξ . The corresponding laminar consumption

rate is calculated by integrating $\psi = |\nabla c| \rho_u(\xi) S_L(\xi)$. The burning intensity is calculated from the ratio of the turbulent and laminar consumption rates.

Figure 3 shows that the laminar consumption rates in cases C1, C4, and C5 differ at the inlet – because the three flames are anchored by flames with $\varphi = 0.7, 1.0$ and 0.41 respectively, but subsequently converge towards the value for the premixed $\varphi = 0.7$ C1 case as the respective flames interact with the mixing layer. This indicates that the flame front in the back-supported C4 case tends to propagate out of the stoichiometric products; to remain at the location where $\varphi = 0.7$; and not to venture further into the fuel-lean mixture where the flame speed falls off rapidly. Conversely, the laminar consumption rate in the front-supported C5 case indicates that the flame propagates from the lean products into mixture with equivalence ratio up to 0.7, but not further. These observations can be explained by considering turbulent flame propagation under the regime of these simulations as a largely passive mixing process between the reactants in the jet and products in the coflow fluid, and then noting that the reaction rate becomes significant only for $\varphi \gtrsim 0.7$.

Figure 3 also shows that the burning intensity in back(front)- supported case C4 (C5) is enhanced (attenuated), compared to the perfectly premixed case C1. Since all three flames C1, C4, and C5 have similar laminar consumption rates (i.e. the instantaneous flame front resides at approximately $\varphi = 0.7$ in all cases) the difference in burning intensity is attributed to differing mean equivalence ratio gradients within the flame brush. Since the local mixture fraction-progress variable alignment necessarily correlates with the mean mixture fraction-progress variable alignment, the observation that back-supported turbulent flames have higher burning intensity than front-supported turbulent flames can be explained by modified transport of heat and radicals from the products into the reaction zone due to the local flame-normal mixture fraction gradient, as observed in previous laminar flame studies [9].

The flame surface area in flames C1, C4 and C5 is similar over the first two jet heights (3.6mm) downstream from the nozzle since the initial flame wrinkling is dominated by the high-intensity turbulent flow imposed at the inlet. From two until six jet heights (10.8mm) downstream of the inlet, the surface areas of flames C1 and C4 continue to increase in a similar manner up to a normalised flame surface area of 3, whereas the normalised surface area of flame C5 levels off at 2. The difference between the higher flame surface area in case C1 and the lower flame surface area in case C5 can be explained by the approximately five-fold lower local consumption speed in the near field of flame C5, which leads to less surface area generation. The local consumption speed in case C4 is a little higher than in case C1, however the near-field flame surface area is very similar and possibly slightly lower on average. This suggests that flame surface area dynamics may depend not only on the mean consumption speed but also on the mixture fraction-progress variable alignment, and this

phenomenon is analysed in detail in a forthcoming publication by these authors. Beyond six jet heights downstream, the two sides of the jet flame start to interact and it is no longer valid to consider two separate flame brushes.

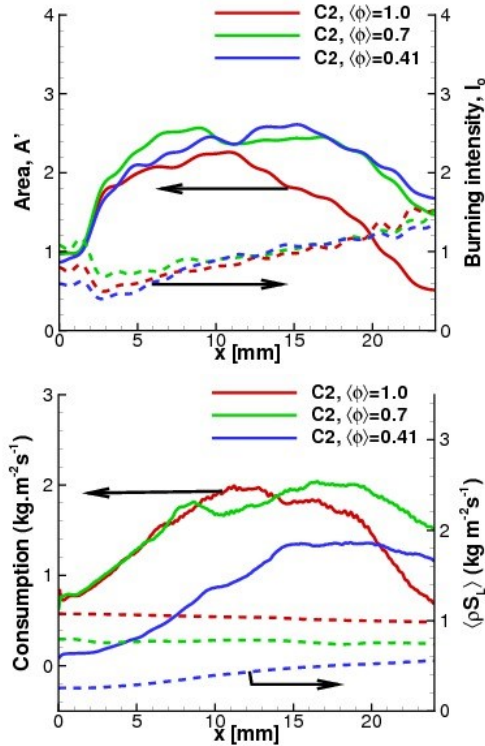


Figure 4. Stream-wise variation of turbulent flame properties in case C2 at three span-wise locations.

Case C2 has a span-wise variation of equivalence ratio imposed on the slot-Bunsen flame and the three span-wise locations presented in Figure 4 correspond to regions where the equivalence ratio is homogeneously equal to 0.41 and 1.0, and an equivalence-ratio stratified region where the mean equivalence ratio equals 0.7. The laminar consumption rate in case C2 depends on the mean equivalence ratio, as shown in Figure 4, and the laminar consumption rate in the mixing layer, where $\phi = 0.7$ is similar to the value in the perfectly premixed C1 case – showing little effect of stratification on the laminar consumption rate. The burning intensity is very similar in the two homogeneous regions, and approximately 20% higher in the stratified region in the near-field – suggesting that the stratified combustion might be relatively more resilient against the weakening effects of strain. The flame surface area is also highest for the stratified mixture over the first six jet heights, resulting in a turbulent consumption rate very close to that in the stoichiometric mixture, despite the lower laminar consumption rate under lean conditions.

The effect of equivalence ratio stratification on flame speed has been investigated further by calculating the conditional average normalised displacement speed ($\rho S_d / \rho_u(\phi)$) and the strain rate tangential to the flame in case C2, conditioned on $\phi = 0.7$, $c = 0.65$ (which is indicative of the location of maximum heat release), and on a range of flame normal mixture fraction gradients

$d\xi/dn$. The flame normal vector $-\nabla c / |\nabla c|$ points towards the reactants, so that a positive value of $d\xi/dn$ indicates that this fuel-lean flame is front supported. The conditionally averaged displacement speed, coloured by the conditionally-averaged tangential strain rate is plotted in Figure 5, and compared with the displacement speed computed from reactant-to-product counter-flow laminar flame calculations with the same equivalence ratio range as case C2 and a range of imposed strain rates.

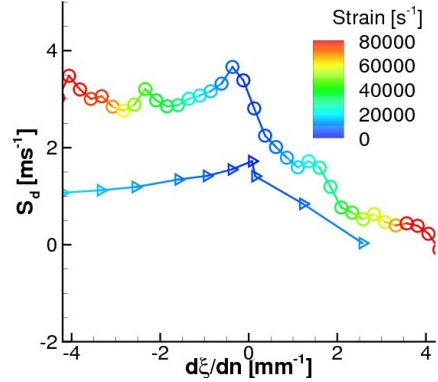


Figure 5. Conditionally-averaged displacement speed versus flame-normal mixture fraction gradient. Circles: case C2 at $x/L_x = 0.5$; Triangles: laminar counter-flow flame data.

The turbulent flame shows higher average displacement speeds and less sensitivity to mean strain than the laminar flame, and this difference may be attributed to the effects of the unsteady variation of strain and flame curvature in the turbulent flame, compared to the stationary planar flame front simulated in the laminar counter-flow. However the displacement speed shows an asymmetrical response to flame normal equivalence ratio gradients in both the laminar and turbulent cases, with back supported flames propagating faster compared to front-supported flames at a given tangential strain rate. The similar dependence of flame speed on flame-normal mixture fraction gradient in both the turbulent and laminar cases suggests that the phenomenon is due to the effect of molecular transport from the products that has been identified previously in laminar flame studies [9].

Figure 6 shows the mixture fraction-progress variable cross-dissipation rate $\chi_{zc} = 2D_\xi \nabla \xi \nabla c$ conditionally averaged on the sample-space variable for mixture fraction, η . The sign of the cross dissipation indicates the orientation of the flame and the mixture fraction gradient (positive values indicate back support). The mean mixture fraction and progress variable gradients are orthogonal at the inlet to case C2, however Figure 6 indicates that there is a tendency for the leaner portion of the flame to develop back-supported alignment with the local mixture fraction gradients. The alignment becomes weaker and slightly front-supported towards the stoichiometric composition, and the magnitude of the conditional mean cross dissipation is always much less than the magnitude of the root-mean-squared fluctuations. The tendency for the lean flame to align in a back-supported orientation may result from the differential propagation mechanism described by Grout et al. [2] and analysed further in a forthcoming publication. The

combined effects of the asymmetric response to flame normal mixture fraction gradients and the preferential back-supported alignment seen in case C2 help to explain the enhanced burning intensity in the stratified region of the flow, relative to the homogenous fluid with $\phi=0.41$ and 1.0.

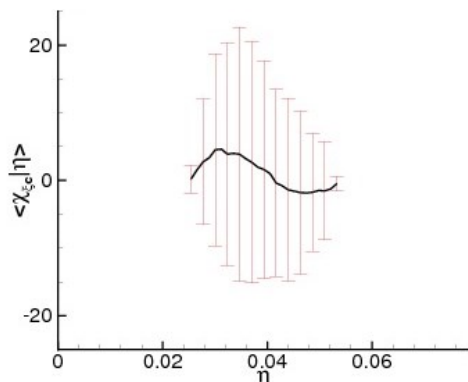


Figure 6. Conditional mean cross dissipation rate \pm the conditional rms versus mixture fraction in case C2 at $x/L_x = 0.5$.

Conclusions

The effects of equivalence ratio-stratification on turbulent flame propagation have been investigated using DNS of methane-air flames with a realistic chemistry model. The orientation of the mean equivalence ratio gradient and the flame brush has a strong effect on the burning intensity within the flame, even controlling for the effect of equivalence ratio at the flame front. It is found that, when the local flame-normal equivalence ratio gradient in the turbulent flame provides ‘back-support’ to the flame front, the local displacement speed is enhanced, whereas the opposite alignment results in slower flame propagation, in agreement with previous observations in laminar flame studies.

Flame surface area generation by differential propagation is expected to be relatively limited in the current DNS due to the high turbulence intensity. The stratification however has a significant influence on the flame surface area due to the variation of the flame surface averaged consumption speed with surface averaged equivalence ratio and equivalence ratio gradient orientation. The differential propagation mechanism however promotes a preferential alignment of the local equivalence ratio gradient with the flame front that depends on the local equivalence ratio. This effect contributes to the average burning intensity and, as a consequence, may feed back to the overall flame surface generation. There is now a need for further analysis of the scaling of front/back-support and differential propagation effects in order to delineate regimes of equivalence ratio-stratified combustion where these effects are significant and may require modelling.

Acknowledgements

This work was supported by the Division of Chemical Sciences, Geosciences and Bio-sciences, the Office of Basic Energy Sciences, the U.S. Department of Energy. Sandia National Laboratories is a multi-program

laboratory operated by Sandia Corporation, a Lockheed Martin Company, for the U.S. Department of Energy under contract DE-AC04-94-AL85000. This research used resources of the National Center for Computational Sciences at Oak Ridge National Laboratory, which is supported by the Office of Science of the U.S. Department of Energy under Contract No. DE-AC05-00OR22725, and the NERSC at Lawrence Berkeley National Laboratory, which is supported by the U.S. Department of Energy under Contract No. DE-AC02-05CH11231. E.S. Richardson is grateful for funding from the Engineering and Physical Science Research Council (UK) (EP/I004564/1).

References

- [1] Driscoll J.F, *Prog. Energy and Comb. Sci.* 34(2008) 91-143.
- [2] Grout RW, Swaminathan N, Cant RS, *Combust. Theor. Model.* 13(5) (2009) 823 – 852.
- [3] D.C. Haworth, R.J. Blint, B. Cuenot and T.J. Poinso, *Combust. Flame* 121 (2000) 395-417.
- [4] C. Jiménez, B. Cuenot, T. Poinso and D. Haworth, *Combust. Flame* 128 (2002)1-21.
- [5] Shreekrishna, Hemchandra S, Lieuwen T, *Combust. Theor. Model.* 14(5) (2010) 681–714.
- [6] Richardson E.S. Knudsen E, Proceedings of the International Workshop on Measurement and Computation of Non-Premixed Flames, Beijing 2010.
- [7] Ramaekers WJS, van Oijen JA, de Goey LPH, *Combust. Theor. Model.* 16 (6) (2012) 943-975.
- [8] Malkeson SP, Chakraborty N, *Flow Turb. Combust.* 90 (2013) 143-187.
- [9] Richardson ES, Granet VE, Eyssartier A, Chen JH, *Combust. Theor, Model.* 14(6)(2010)775-792.
- [10] Richardson, E.S., Sankaran, R., Grout, R.W., Chen, J.H., *Combust. Flame*, 157(3)(2010), 506-515.
- [11] Sankaran R, Hawkes, E.R., Yoo, C.S., Chen, C.S. Lu, T. Law, C.K., in *5th US National Combustion Meeting*, (2007) B09.
- [12] Sankaran R, Hawkes ER, Chen JH, Lu T, Law CK, *Proc. Combust. Inst.* 31(1)(2007)1291-1298.
- [13] Passot T, Pouquet A, *J. Fluid Mech.* 181 (1987) 441-466.
- [14] Smooke MD, Giovangigli, V., in: M.D. Smooke (Ed.), *Lect. Notes Phys.* 284 (1991) 1-28.
- [15] Chen JH, Choudhary A, de Supinski B, DeVries M, Hawkes ER, Klasky S, Liao WK, Ma KL, Mellor-Vrummy J, Podhorszki N, Sankaran R, Shende S, Yoo CS, *Computational Science & Discovery* 2(2009)015001.
- [16] Kennedy CA, Carpenter MH, *Appl. Numer. Math.* 14(4)(1994) 397-433.
- [17] Kennedy CL, Crpenter MH, Lewis RM, *Appl. Numer. Math.* 35(2000)177-219.
- [18] Yoo CS, Im HG, *Combust. Theor. Model.* 11(2)(2007)259-286.
- [19] Peters N, *Turbulent combustion*. Cambridge University Press, Cambridge, UK, 2000.